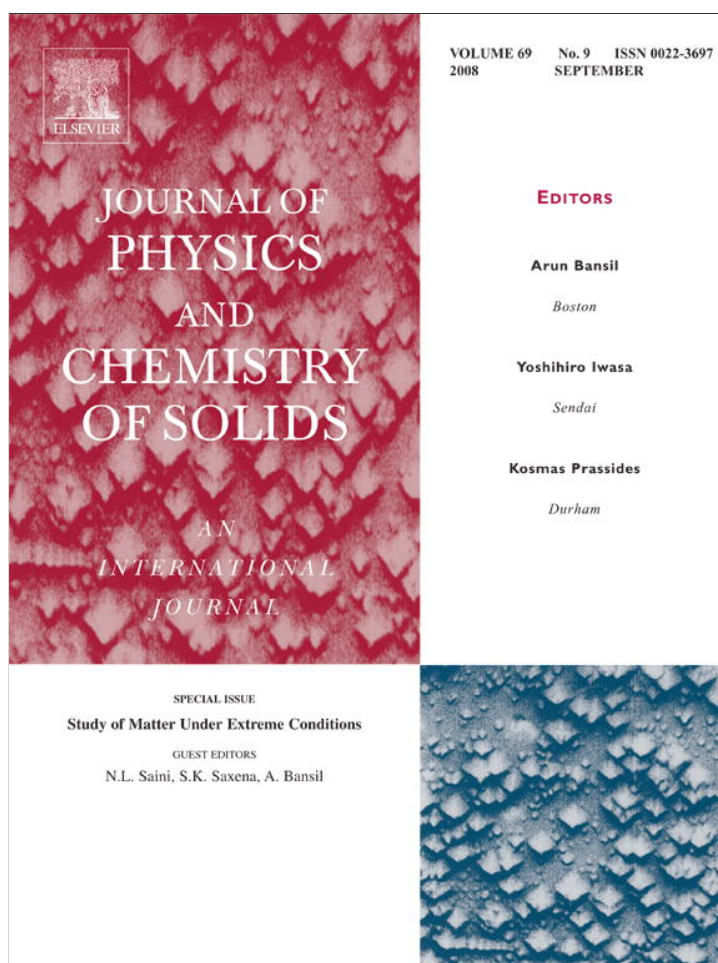


Provided for non-commercial research and education use.
Not for reproduction, distribution or commercial use.



This article appeared in a journal published by Elsevier. The attached copy is furnished to the author for internal non-commercial research and education use, including for instruction at the authors institution and sharing with colleagues.

Other uses, including reproduction and distribution, or selling or licensing copies, or posting to personal, institutional or third party websites are prohibited.

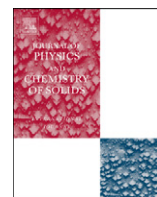
In most cases authors are permitted to post their version of the article (e.g. in Word or Tex form) to their personal website or institutional repository. Authors requiring further information regarding Elsevier's archiving and manuscript policies are encouraged to visit:

<http://www.elsevier.com/copyright>



Contents lists available at ScienceDirect

Journal of Physics and Chemistry of Solids

journal homepage: www.elsevier.com/locate/jpcs

Melting curve of silicon to 15 GPa determined by two-dimensional angle-dispersive diffraction using a Kawai-type apparatus with X-ray transparent sintered diamond anvils

Atsushi Kubo^{a,1}, Yanbin Wang^b, Claire E. Runge^a, Takeyuki Uchida^b, Boris Kiefer^c, Norimasa Nishiyama^{b,2}, Thomas S. Duffy^{a,*}

^a Department of Geosciences, Princeton University, Princeton, NJ 08544, USA

^b Center for Advanced Radiation Sources, University of Chicago, Chicago, IL 60637, USA

^c Department of Physics, New Mexico State University, Las Cruces, NM 88003, USA

ARTICLE INFO

Keywords:

C. High pressure
C. X-ray diffraction
D. Phase transitions
D. Phase equilibria

ABSTRACT

The melting curve of silicon has been determined up to 15 GPa using a miniaturized Kawai-type apparatus with second-stage cubic anvils made of X-ray transparent sintered diamond. Our results are in good agreement with the melting curve determined by electrical resistivity measurements [V.V. Brazhkin, A.G. Lyapin, S.V. Popova, R.N. Voloshin, Nonequilibrium phase transitions and amorphization in Si, Si/GaAs, Ge, and Ge/GaSb at the decompression of high-pressure phases, *Phys. Rev. B* 51 (1995) 7549] up to the phase I (diamond structure)—phase II (β -tin structure)—liquid triple point. The triple point of phase XI (orthorhombic, *Imma*)—phase V (simple hexagonal)—liquid has been constrained to be at 14.4(4) GPa and 1010(5) K. These results demonstrate that the combination of X-ray transparent anvils and monochromatic diffraction with area detectors offers a reliable technique to detect melting at high pressures in the multianvil press.

© 2008 Elsevier Ltd. All rights reserved.

1. Introduction

Although at least eight high-pressure crystalline phases have been discovered in Si under pressure up to 248 GPa at room temperature (e.g. [1]), many aspects of the phase diagram of Si remain unknown as few experiments have been carried out at simultaneous high pressure and temperature. Si has a cubic diamond structure (phase I) at ambient conditions. By quasi-hydrostatic compression at room temperature, it transforms into a tetragonal β -tin structure (phase II) at 11–12 GPa [2,3], a body-centered orthorhombic (*Imma*) structure at 14.4 GPa (phase XI) [3,4], and a simple hexagonal structure (phase V) at 15.4 GPa [3]. A review of high-pressure phases of Si is given in [5].

The melting curve of Si has been studied using differential thermal analysis [6,7] and resistivity measurements [8,9]. Since the liquid (L) phase of Si is denser than phase I, the melting temperature decreases with pressure up to the I–II–L triple point

(e.g. [6]). In these studies, melting temperatures could be precisely determined by monitoring changes in temperature or electrical conductivity *in situ*. However, pressures may contain large uncertainties (except for the study by [6], who used a piston cylinder device) because pressures at high temperatures were assumed to be identical to those at room temperature estimated from hydraulic ram loads using a calibration curve. The calibration curve was established prior to the experiments from fixed pressure points that were defined by certain phase transitions in metals and semiconductors such as Bi. The phase relations in Si at simultaneous high pressure and temperature were examined by *in situ* energy-dispersive X-ray diffraction using a Kawai-type apparatus (called as “T-cup”) up to 15.5 GPa and 1073 K [10]. Although a melting point of phase XI was reported to be 12.7 GPa and 1053 K, they mainly focused on solid phase boundaries. The melting curve of Si has been predicted up to 15 GPa from thermodynamic calculations [11] and from the atomistic simulations [12] with the tight-binding model. The former gives consistent results with the electrical resistivity measurements [8], while the latter reports that melting temperatures at room temperature and at ~ 11 GPa are ~ 100 K lower and ~ 300 K higher than those experimentally reported [10], respectively.

To make an accurate determination of the melting curve, we have developed a two-dimensional (2D) angle-dispersive setup

* Corresponding author. Tel.: +16092586769; fax: +16092681274.

E-mail address: duffy@princeton.edu (T.S. Duffy).

¹ Now at: Superhard Materials Development Dept., Sumitomo Electric Hard-metal Corp., Itami, Hyogo, 664-0016, Japan.

² Now at: Geodynamics Research Center, Ehime University, Matsuyama, Ehime 790-8577, Japan.

with a miniaturized Kawai-type high-pressure apparatus, which permits much greater number of grains present in the sample compared to an energy-dispersive setup. Angle-dispersive geometry allows detection of complete Debye–Scherrer rings, whereas the energy-dispersive geometry only samples a small azimuth range along the ring. Therefore, the number of crystal grains whose diffraction can be detected by energy-dispersive setup is significantly lesser than that observed by angle-dispersive setup. In general, the sample just before melting and after solidification tends to show a highly textured diffraction pattern without Debye–Scherrer rings but with just a few diffraction spots due to re-crystallization. These diffraction spots can appear at any azimuth angle. If energy-dispersive setup is used [10], one could easily underestimate the melting temperature. Also, the use of angle-dispersive geometry allows for observation of diffuse scattering from the liquid. Here we report details of this newly developed experimental setup and the results on melting curve and solid phase boundaries of Si up to 15 GPa.

2. Experimental procedure

We used X-ray transparent sintered diamond anvils as an X-ray window with a T-10 module [13], which allows us to record complete Debye–Scherrer rings over a 2θ range up to 10° . With high-energy (65 keV) monochromatic X-rays, a 2θ value of 10° corresponds to d -spacing of $\sim 1.1 \text{ \AA}$ or $Q (= 4\pi \sin \theta / \lambda)$ of $\sim 5.7 \text{ \AA}^{-1}$. The first stage of the T-10 module consists of a set of six wedges, which are cut from a 120 mm diameter high-strength steel cylinder. Each wedge has an $18 \times 18 \text{ mm}^2$ square truncation, and the six wedges are divided into two groups of three wedges, both groups of which are mounted in a confinement ring, forming an upper and lower guide block. The first-stage wedges have $\pm 10^\circ$ semi-conical notches, which define the 2θ range for X-ray access. Eight sintered WC cubes are typically used as the second-stage anvils. Each of these 10 mm edge-length cubes has a triangular truncation at the corner so that when the eight cubes are assembled, an octahedral cavity is formed at the center, within which the sample assembly is compressed. The edge length of the triangular truncation used in this study is 2.0 mm. The eight-cube assembly is compressed in the first-stage wedges by a hydraulic ram in the vertical direction, along the (111) axis of the cubic assembly. Pressures and temperatures up to 25 GPa and 2000 K, respectively, have been reached with a hydraulic ram load of about 150 T [14].

When two WC anvils located on the downstream side are replaced with X-ray transparent anvils, diffraction signals from a $\pm 10^\circ$ solid angle can be collected by the angle-dispersive method (Fig. 1). To test our ability to record X-ray diffraction signals through these anvils, we conducted X-ray absorption measurements on anvils composed of polycrystalline cubic boron nitride (cBN) and sintered diamond with either Si (Si-SD) or Co (Co-SD) as binding agents. The tests were performed using comparative X-ray radiography with a monochromatic incident X-ray beam of 60 keV with a charge-coupled device (CCD) detector. For 10-mm-thick materials, both Si-SD and cBN cubes reduced intensity by

about 50%, while the Co-SD cube reduced intensity by more than 90%. Therefore, it is realistic to collect monochromatic diffraction patterns through the Si-SD or cBN cubes rather than Co-SD.

High-pressure melting experiments were conducted in the 250-T multianvil press at the bending magnet beamline 13-BM-D of Advanced Photon Source at Argonne National Laboratory [15,16]. Monochromatized X-rays at 65 keV with a dimension of $100 \times 100 \mu\text{m}^2$ were directed onto the sample. Diffracted X-rays were detected with a Bruker SMART 1500 X-ray CCD that has 1024×1024 pixels and a nominal pixel size of 0.09 mm. We used two Si-SD anvils (DIACOM[®], Ringwood Superabrasives Pty Ltd, Australia) as X-ray windows. The cell assembly was similar to that of [14], which used two sheet heaters made of TiC+diamond powder (Fig. 2). The pressure medium was made of mullite to improve thermal insulation and contained an X-ray window on the down-stream side made of a mixture of amorphous boron and epoxy resin (BE). The gasket between the two Si-SD anvils was also made of BE to obtain a smooth background in diffraction data. The cell assembly had two sample chambers that are symmetric with respect to the thermocouple junction (Fig. 2). Silicon powder (99.999%, Alfa Aesar) was mixed with hexagonal BN (hBN) powder (99.5%, Alfa Aesar) in a ratio of 5:7 by weight to suppress grain growth in Si. The sample mixture was loaded in one chamber, and a mixture of Au and MgO powders with a mixing ratio of 1:10 by weight was in the other. A sample capsule made of hBN (grade HBC, oxygen 0.081%, GE Advanced Ceramics) was placed around the Si+hBN to prevent chemical reaction between Si and the BE pressure medium (Fig. 2). Temperature was measured using a W95/Re5-W74/Re26 thermocouple. Temperature variation during heating was within $\pm 5 \text{ K}$ except in the final heating cycle at $\sim 3 \text{ GPa}$, where it was $\pm 10 \text{ K}$. By moving the press position relative to the fixed X-ray path, we collected diffraction data for Si+hBN and MgO+Au separately. Pressures were determined from the thermal equations of state of MgO [17] and Au [18]. We used Au as a primary pressure scale because Au is expected to have less differential stress at high temperature than MgO, due to its lower rigidity and melting temperature compared to MgO. To calculate unit cell volumes of these materials, 200 and 220 reflections were used for MgO, while 111 and 200 reflections were used for Au. Lattice parameters of high-pressure phases of Si were calculated from 020, 011, 220, 121, and 031 reflections of phase II, 200, 020, 011, 220, and 211 reflections of phase XI, and 001, 010, 011, and 110 of phase V.

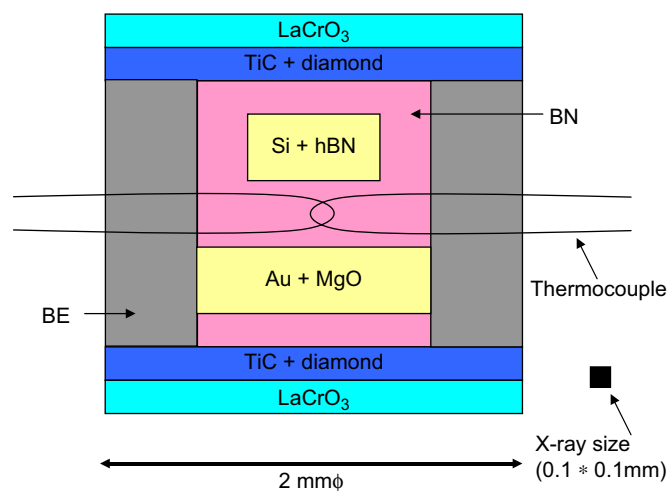


Fig. 2. Cross-section of the sample chamber placed in an octahedral pressure medium. BE—amorphous boron and epoxy resin. LaCrO_3 plate was placed outside the TiC+diamond heater for better thermal insulation.

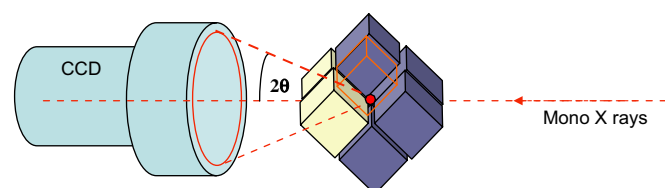


Fig. 1. Diffraction geometry of angle-dispersive setup using Kawai-type apparatus with two Si-SD anvils as X-ray windows.

2D diffraction data were integrated over the entire 360° azimuth angle using the software Fit2d [19] to yield 1D intensity versus 2θ patterns. The tilt and rotation of the X-ray CCD were corrected using a CeO_2 standard at ambient conditions. The detector–sample distance (~ 270 mm) was calibrated before and after the experiment using MgO, Au, and Si inside the cell assembly in the T-10 module. The distances derived from Au, MgO, and Si were all consistent: 270.75 mm from Si, 270.73 mm from Au, and 270.69 mm from MgO before compression;

270.49 mm from Au and 270.58 mm from MgO after compression. Therefore, we infer that the detector–sample distance did not change by more than 0.2 mm during the experiments, and the associated uncertainty in pressures due to uncertainty of detector–sample distance is up to ± 0.25 GPa for Au and MgO.

Below 1000 K, we sometimes observed azimuthal dependence in the d -values in the 2D diffraction data. This modulation is due to differential stress in the sample. The direction of X-rays is perpendicular to the axis of the cylindrical sample chamber in

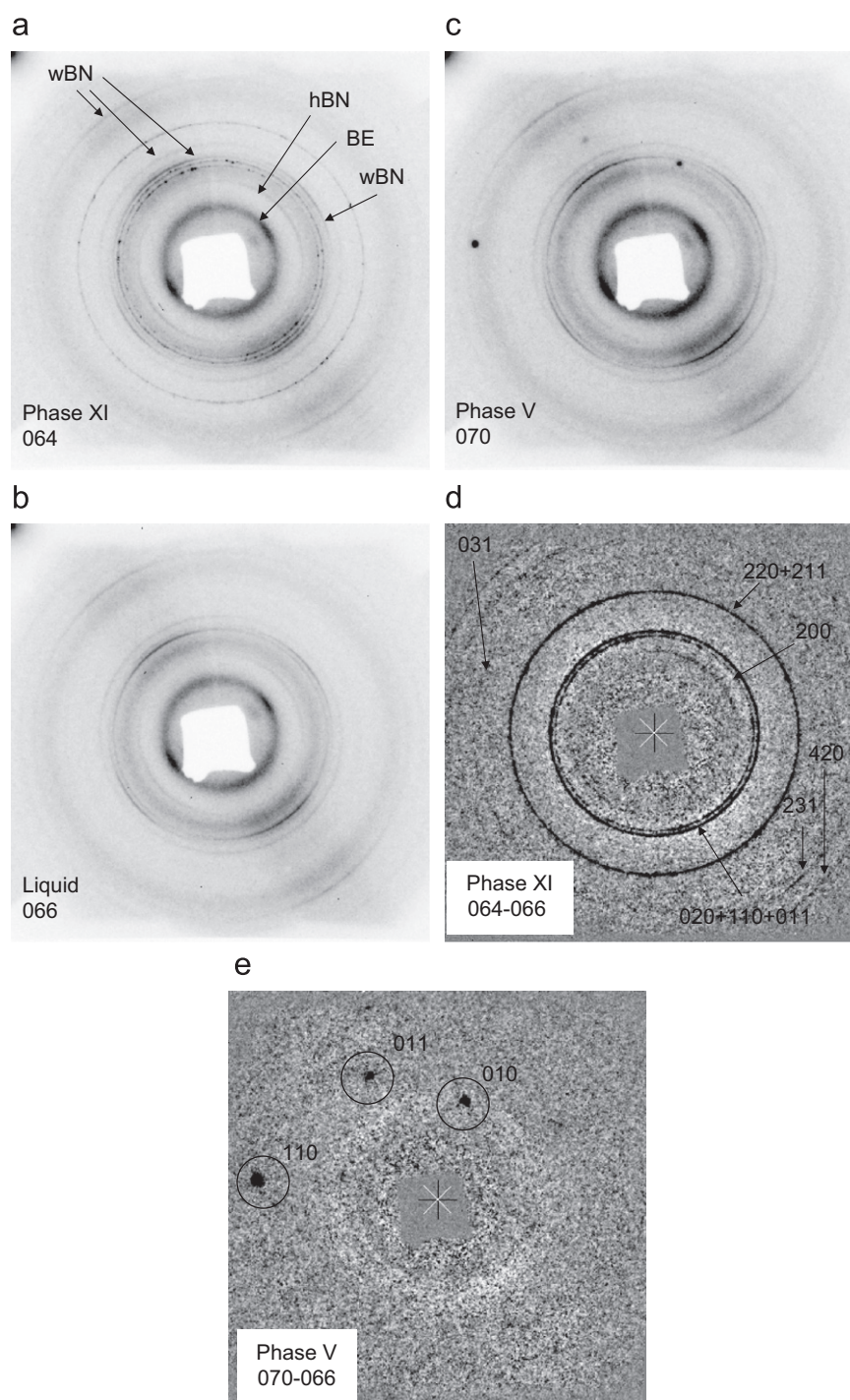


Fig. 3. 2D diffraction patterns of Si collected in the first heating cycle at 80 tons. Raw 2D diffraction data are (a) phase XI before melting, (b) liquid, and (c) phase V after solidification. Background-subtracted 2D data are (d) phase XI and (e) phase V, in which 2D data after melting (b) was used as a background. See (d) and (e) for identification of Debye–Scherrer rings from phase XI in (a) and from phase V in (c), respectively. Asterisk in (d,e) represents the position of direct X-ray beam. The higher background (shadow) from left top to right bottom in (a–c) is caused by the anvil gap, where the absorption of X-rays by the anvil material is absent. Such background structure can be erased by the background subtraction (d,e).

which an axially symmetric stress field can be reasonably assumed as a first approximation (see Fig. 2b in [14]). According to lattice strain theory [20], one can estimate d -values that are free from the effect of differential stress from some specific azimuth angles in the 2D data (referred to as the magic angles). Data integration from magic angles, where the directions of diffracting plane normal are $\sim 55^\circ$ away from the direction of unique principle stress, yielded pressures that are up to 1 GPa higher than those obtained from whole angle integration. Above about 1000 K, azimuthal dependence in the d -values was insignificant, and pressures determined from magic angle integration were consistent with those from whole pattern integration.

Detection of melting was initially made by observation of disappearance of all diffraction rings or spots of Si from the 2D data, but finally confirmed by observation of diffuse scattering in the diffraction data after background subtraction. In the angle-dispersive setup, the shape of the background strongly depends on the relative position relationship of X-ray beam and components of the high-pressure cell, including the gasket. Since the cell continuously deforms during the experiment, which changes the shape of the background, it is not feasible to obtain a universal background applicable to all experimental data. We found that the diffraction data obtained just before melting and after solidification contain the best background information, the most suitable for background subtraction during melting.

Representative 2D X-ray diffraction/scattering data of Si during experiments are shown in Figs. 3a–c, which also contain Debye–Scherrer rings from hBN and wurtzite-type BN and a background (diffuse scattering) from the BE pressure medium and gasket. By using the diffraction datum before melting or after solidification as a representative background (e.g. Fig. 3c), one can subtract the background from the datum during melting (Fig. 3b) to extract the diffuse scattering from the liquid (Fig. 4). Such a procedure yields a subtracted pattern that contains artifacts from diffraction peaks (Fig. 4). This is because the peak intensity of BN is always changing by time during heating due to phase transformation from hBN to wBN. Also, crystal growth of one phase or another, even without phase transformation, could also produce such effects. By using the diffraction pattern during melting as a background (Fig. 3b), one can also make background subtraction from the data before melting or after solidification (Figs. 3a and c) to extract diffraction pattern from the sample (Figs. 3d and e). In both methods, diffuse scattering from Si melt can be recognized as a halo around the 020 ring of phase XI

(Fig. 3d) and the 010 ring of phase V (Fig. 3e). In Fig. 4, diffuse scattering from Si melt can be clearly seen at 2θ values between 4° and 6° , demonstrating robustness of this experimental method in detecting melting.

By increasing both photon energy and 2θ range, decreasing sample–detector distance for higher Q coverage, and removing artifacts, it may be possible to use this technique to determine melt structure.

3. Results

A total of six melting–solidification cycles were conducted at various fixed loads. In the first heating cycle at 80 T, formation of phase II ($a = 4.6883$ (4) Å, $c = 2.6023$ (5) Å) was confirmed at 673 K and 15.5(5) GPa, coexisting with phase I. At 873 K, pressure dropped to 14.4(5) GPa and only phase II ($a = 4.692$ (2) Å, $c = 2.608$ (2) Å) was observed. According to the results by [3,10], phases I and II are metastable in this pressure range. Phase XI was then observed at 14.3(4) GPa and 923 K ($a = 4.751$ (5) Å, $b = 4.616$ (5) Å, $c = 2.606$ (4) Å) and 973 K ($a = 4.783$ (8) Å, $b = 4.577$ (9) Å, $c = 2.611$ (6) Å). The entire Debye–Scherrer rings were observed so far for all the Si phases (Fig. 3a). At 14.6(4) GPa and 1048 K, all Debye–Scherrer rings from Si disappeared, and diffuse scattering was observed after background subtraction (Figs. 3d and 4). On cooling to 998 K, three diffraction spots from phase V ($a = 2.615$ (2) Å, $c = 2.416$ (5) Å) appeared at 14.5(4) GPa (Fig. 3c). After quenching to room temperature at 11.8(4) GPa, only diffraction spots from phase II were observed.

The second heating cycle was also made at 80 T. We observed diffraction spots from phase II up to 573 K and 12.9 (4) GPa. Diffraction spots from phase XI were then observed between 673 and 13.3 (4) GPa, constraining a II–XI phase boundary between these conditions. Phase XI was observed up to 973 K and 14.5(4) GPa. At 993 K and 14.5(4) GPa, diffraction spots from phase V were observed. The sample then melted at 1013 K and 14.6(4) GPa. After solidification, diffraction spots from phase XI were observed at 983 K, 14.5(4) GPa. These two heating cycles were made at conditions very close to the triple point of phase XI–V–L, providing a tight constraint on the XI–V phase boundary between 983 and 993 K at 14.5(4) GPa and a melting point of phase V at 14.6(4) GPa between 998 and 1013 K.

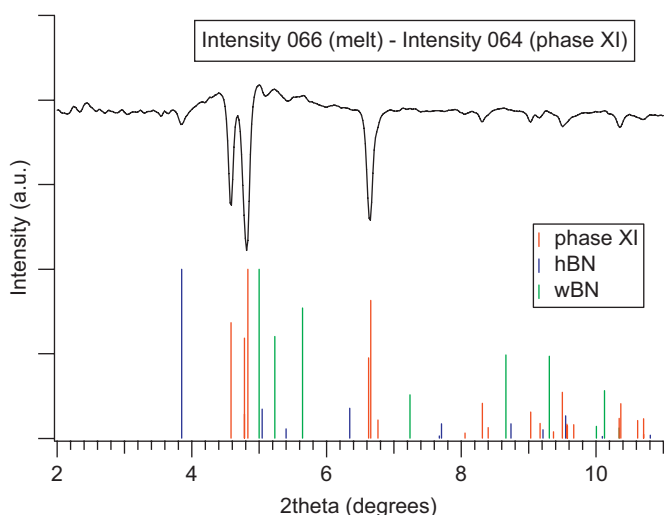


Fig. 4. A representative 1D diffraction data of liquid after background subtraction.

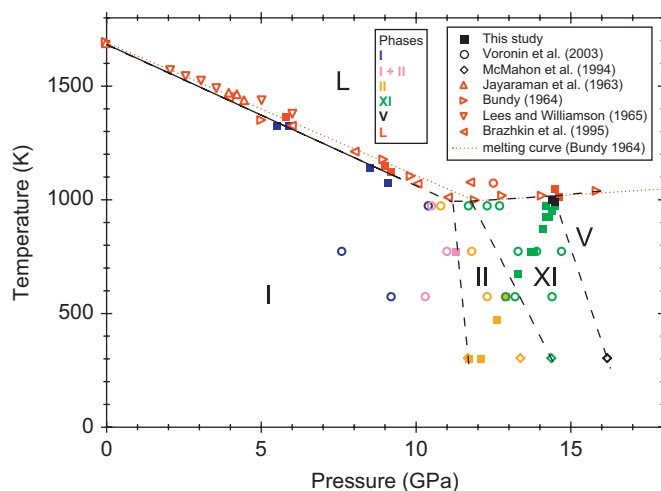


Fig. 5. Phase diagram of Si inferred from the results of both the present study and McMahon et al. [3]. Also shown are in situ X-ray diffraction results after Voronin et al. [10] during isothermal compression and melting points reported by Jayaraman et al. [6], Bundy [8], Lees and Williamson [7], and Brazhkin et al. [9]. Colors and shapes of the symbols represent phases and source data, respectively.

Similar heating cycles were repeated at 25, 17, and 10 T, starting from the stability field of phase I (Fig. 5). To reach each pressure step, hydraulic load was reduced at a constant temperature of 773 K. During decompression from 80 to 25 T, we observed back transformation from phase XI to a mixture of phase I+II at 11.3(4) GPa, which should constrain the I–II phase boundary at 773 K. In the fifth heating cycle at 10 T, we detected melting at 1413 K, while in the sixth cycle at 10 T it was detected again at 1403 K, showing excellent reproducibility. However, pressures determined from Au and MgO were only marginally consistent: 3.2(4) and 3.9 (3) GPa, respectively, at 1413 K. Accurate pressure determination from Au and/or MgO at very low pressures and high temperatures, where relative volumes V/V_0 are close to 1 or higher, may be challenging, as discussed by [21] for MgO. Therefore, we did not use these melting data at 10 T to constrain melting curve of Si (Fig. 5).

4. Discussion

Before the start of the melting experiment, Si was compressed at 673 K between 8 and 12 GPa and then compressed to 15 GPa at room temperature. During this process, we should have crossed the I–II phase boundary according to the results by [10], but we never observed phase II. There are no previous experimental studies that reported stability of Si-I above 12 GPa, and the I–II transition pressure is known to be reduced by the application of differential stress [2]. The I–II transition has been predicted to be kinetically very difficult (e.g. [22]), and has been experimentally reported to be very sluggish, requiring a ~ 3 GPa overpressure to complete the phase transition at room temperature [10]. We infer that the reason for our observation of phase I at such a great overpressure is due to hot compression of Si at 673 K, which could reduce both defect concentration and differential stress in the sample, resulting in metastable presence of low-pressure phases under greater overpressure [23]. Phase II, observed as a result of transition from phase I during first heating at ~ 15 GPa, may also be a metastable phase because the observation of phase II here is not consistent with the observation of phase XI transformed from phase II in the second heating cycle at lower pressures. Therefore, our observation implies that a phase transition from phase I to phase II is kinetically more favorable than a direct transition from phase I to phase XI at 673 K.

Fig. 5 shows the phase diagram of Si up to 15 GPa determined in the present study. The melting curve up to ~ 9 GPa was estimated from two melting points at ~ 6 and ~ 9 GPa together with the known melting point of Si at ambient pressure and 1683 K (e.g. [6]). The melting curve can be expressed by T (K) = $-62.3 (1.4)P$ (GPa) + 1683, and is generally consistent with previous experimental studies [6–10]. In particular, it is in excellent agreement with that of Brazhkin et al. [9] up to the I–II–L triple point reported by these authors at 11 GPa and 1000 K. Our results also place a tight constraint on the XI–V–L triple point, which is estimated to be 14.4(4) GPa and 1010(5) K, as explained earlier.

The pressure scales and pressure vessels used in previous experimental studies of Si melting are listed in Table 1. Bundy [8] calibrated his belt apparatus at room temperature using resistance transitions in Bi (2.5 GPa), Ba (5.8 GPa), Bi (8.8 GPa), Fe (13.0 GPa), Eu (15.0 GPa), and Pb (16.1 GPa). These transition pressures are different from those approved by National Bureau of Standards (NBS) in 1968 (2.55, 5.5, 7.7, 11.0–11.3, 12.2–13.0, and 12.8–13.2 GPa for Bi, Ba, Bi, Fe, Eu, and Pb, respectively). Since the pressure scales used in the present study is more consistent with NBS scales than those used by Bundy [8], it is likely that the inconsistency between melting curves determined in the present

Table 1
Silicon melting studies at high pressures

Reference	Pressure standard (s)	Apparatus
Voronin et al. [10]	NaCl [24]	Kawai type
McMahon et al. [3]	Ruby [25]	Diamond cell
Jayaraman et al. [6]	Fixed point—Bi	Piston–cylinder
Bundy [8]	Fixed pts.—Bi, Ba, Fe, Eu, Pb	Belt
Lees and Williamson [7]	Fixed pts.—Bi, Ti, Ba	Tetrahedral anvil
Brazhkin et al. [9]	Fixed pts.—Bi, Ba, Pb	Toroidal anvil

study and by Bundy is related to the differences in resistance transition pressures.

Whereas our results are insufficient to constrain phase boundaries between I–II, II–XI, XI–V, triple points of I–II–L, II–XI–L, and the melting curve above the I–II–L triple point, we can suggest these locations by combining our results with experimental data of McMahon et al. [3]. The topology of the proposed phase diagram (Fig. 5) is consistent with that by Voronin et al. [10], but the I–II and II–XI phase boundaries suggested in the present study locate at positions that are up to 1.5 GPa higher than those proposed in [10]. A possible XI–V phase boundary can be expressed as a tie line between the XI–V–L triple point and a data point at 16.2(1) GPa and room temperature where the onset of XI–V phase transition was observed by [3]. A possible I–II boundary can be suggested as the line that contains both the datum at 11.7(1) GPa and room temperature, where the onset of I–II phase transition was observed by [3] and the datum at 11.3(4) GPa and 773 K, where the onset of II–I phase transition was observed during decompression in the present study. This phase boundary intersects with the melting curve of phase I at 11.2(5) GPa and 985(30) K to yield the I–II–L triple point. By connecting this triple point and the XI–V–L triple point, the approximate location of the melting curve above the I–II–L triple point can be estimated, which is apparently consistent with that of Bundy [8] in spite of inconsistency in pressure scales discussed above. This apparent consistency is due to gradual slope of the melting curve above the I–II–L triple point (Fig. 5). The II–XI phase boundary can be suggested as the line that contains the datum at 14.4(1) GPa and room temperature in [3] and the midpoint of two adjoining data points at 12.9(4) GPa, 573 K and 13.3(4) GPa, 673 K, where phase II and phase XI, respectively, were observed during the second heating at 80 T. This phase boundary intersects with the melting curve of phases II and XI to yield the triple point of II–XI–L at 11.8(5) GPa and 985(30) K. All these proposed phase boundaries are shown by broken lines in Fig. 5.

The melting curve above the I–II–L triple point heavily relies on the location of the I–II–L triple point. The location of this triple point has been proposed at 12 GPa and 1000 K by Bundy [8], 11 GPa and 1000 K by Brazhkin et al. [9], 10.5(2) GPa and 1003(20) K by Voronin et al. [10], and 11.5 GPa and 950 K by Yang et al. [11]. Precise determination of the location of the I–II–L triple point remains important to validate the melting curve of Si proposed in the present study up to 15 GPa.

Acknowledgments

We thank John Vermynen, Sutatcha Hongsresawat, and GSECARS personnel for their assistance. Comments by an anonymous reviewer greatly improved the manuscript. This work was supported by the NSF and Carnegie–DOE alliance center. GSECARS is supported by the National Science Foundation–Earth Sciences (EAR-0217473), Department of Energy–Geosciences (DE-FG02-94ER14466), and the State of Illinois. Use of the APS was supported by the US Department of Energy, Office of Science,

Office of Basic Energy Sciences, under Contract no. W-31-109-ENG-38. N.N. was partly supported by Postdoctoral Fellowships for Research Abroad of Japan Society for the Promotion of Science.

References

- [1] S.J. Duclos, Y.K. Vohra, A.L. Ruoff, Experimental study of the crystal stability and equation of state of Si to 248 GPa, *Phys. Rev. B* 41 (1990) 12021.
- [2] J.Z. Hu, L.D. Merkle, C.S. Menoni, I.L. Spain, Crystal data for high-pressure phases of silicon, *Phys. Rev. B* 34 (1986) 4679.
- [3] M.I. McMahon, R.J. Nelmes, N.G. Wright, D.R. Allan, Pressure dependence of the Imma phase of silicon, *Phys. Rev. B* 50 (1994) 739.
- [4] M.I. McMahon, R.J. Nelmes, New high-pressure phase of Si, *Phys. Rev. B* 47 (1993) 8337.
- [5] A. Mujica, A. Rubio, A. Munoz, R.J. Needs, High-pressure phases of group-IV, III–V, and II–VI compounds, *Rev. Mod. Phys.* 75 (2003) 863.
- [6] A. Jayaraman, W. Klement, G.C. Kennedy, Melting and polymorphism at high pressures in some group IV elements and III–V compounds with the diamond/zincblende structure, *Phys. Rev.* 130 (1963) 540.
- [7] J. Lees, B.H.J. Williamson, Combined very high pressure/high temperature calibration of the tetrahedral anvil apparatus, fusion curves of zinc, aluminum, germanium, and silicon to 60 kilobars, *Nature* 208 (1965) 278.
- [8] F.P. Bundy, Phase diagram of silicon and germanium to 200 kbar, 1000 °C, *J. Chem. Phys.* 41 (1964) 3809.
- [9] V.V. Brazhkin, A.G. Lyapin, S.V. Popova, R.N. Voloshin, Nonequilibrium phase-transitions and amorphization in Si, Si/GaAs, Ge, and Ge/GaSb at the decompression of high-pressure phases, *Phys. Rev. B* 51 (1995) 7549.
- [10] G.A. Voronin, C. Pantea, T.W. Zerda, L. Wang, Y. Zhao, In situ X-ray diffraction study of silicon at pressures up to 15.5 GPa and temperatures up to 1073 K, *Phys. Rev. B* 68 (2003) 020102.
- [11] C.C. Yang, J.C. Li, Q. Jiang, Temperature–pressure phase diagram of silicon determined by Clapeyron equation, *Solid State Commun.* 129 (2004) 437.
- [12] M. Kaczmarzski, O.N. Bedoya-Martínez, E.R. Hernandez, Phase diagram of silicon from atomistic simulations, *Phys. Rev. Lett.* 94 (2005) 095701.
- [13] Y. Wang, G. Shen, M.L. Rivers, High pressure research at third generation synchrotron sources, in: D. Mills (Ed.), *Third Generation Synchrotron Sources*, Wiley, New York, 2002, p. 203.
- [14] T. Uchida, Y. Wang, M.L. Rivers, S.R. Sutton, Stability field and thermal equation of state of epsilon-iron determined by synchrotron X-ray diffraction in a multianvil apparatus, *J. Geophys. Res.* 106 (2001) 21799.
- [15] Y. Wang, M. Rivers, T. Uchida, P. Murray, G. Shen, S. Sutton, J. Chen, Y. Xu, D. Weidner, High pressure research using large-volume presses at GeoSoilEnviroCARS, Advanced Photon Source, in: *Proceedings of the International Conference on High Pressure Science and Technology (AIRAPT-17)*, Science and Technology of High Pressure, 2000, p. 1047.
- [16] T. Uchida, Y. Wang, M.L. Rivers, S.R. Sutton, D.J. Weidner, M.T. Vaughan, J. Chen, B. Li, R.A. Secco, M.D. Rutter, H. Liu, A large-volume press facility at the Advanced Photon Source: diffraction and imaging studies on materials relevant to the cores of planetary bodies, *J. Phys.: Condens. Matter* 14 (2002) 11517.
- [17] S. Speziale, C.S. Zha, T.S. Duffy, R.J. Hemley, H.K. Mao, Quasi-hydrostatic compression of magnesium oxide to 52 GPa: implications for the pressure–volume–temperature equation of state, *J. Geophys. Res.* 106 (2001) 515.
- [18] S.H. Shim, T.S. Duffy, K. Takemura, Equation of state of gold and its application to the phase boundaries near 660 km depth in Earth's mantle, *Earth Planet. Sci. Lett.* 203 (2002) 729.
- [19] A.P. Hammersley, S.O. Svensson, M. Hanfland, A.N. Fitch, D. Häusermann, Two-dimensional detector software: from real detector to idealized image or two-theta scan, *High Pressure Res.* 14 (1996) 235.
- [20] A.K. Singh, The lattice strains in a specimen (cubic system) compressed nonhydrostatically in an opposed anvil device, *J. Appl. Phys.* 73 (1993) 4278.
- [21] M.J. Walter, T. Katsura, A. Kubo, T. Shinmei, O. Nishikawa, E. Ito, C. Leshner, K. Funakoshi, Spinel–garnet lherzolite transition in the system CaO–MgO–Al₂O₃–SiO₂ revisited: an in situ X-ray study, *Geochim. Cosmochim. Acta* 66 (2002) 2109.
- [22] G.J. Ackland, High-pressure phases of group IV and III–V semiconductors, *Rep. Prog. Phys.* 64 (2001) 483.
- [23] T. Katsura, H. Yamada, T. Shinmei, A. Kubo, S. Ono, M. Kanzaki, A. Yoneda, M.J. Walter, E. Ito, S. Urakawa, K. Funakoshi, W. Utsumi, Post-spinel transition in Mg₂SiO₄ determined by high P–T in situ X-ray diffractometry, *Phys. Earth Planet. Inter.* 136 (2003) 11.
- [24] D.L. Decker, High-pressure equation of state for NaCl, KCl, and CsCl, *J. Appl. Phys.* 42 (1971) 3239.
- [25] G.J. Piermarini, S. Block, J.D. Barnett, R.A. Forman, Calibration of the pressure dependence of the R₁ ruby fluorescence line to 195 kbar, *J. Appl. Phys.* 46 (1975) 2774.